Frontiers in Heat and Mass Transfer (FHMT), 5, 13 (2014)
DOI: 10.5098/hmt.5.13

Global Digital Central
ISSN: 2151-8629

Frontiers in Heat and Mass Transfer

Available at www.ThermalFluidsCentral.org

A DRYING AND THERMOELASTIC MODEL FOR FAST MICROWAVE HEATING OF CONCRETE

Benjamin Lepers[a,*], Aditya Putranto[b,c], Martin Umminger[d], Guido Link[a], John Jelonnek[a]

[a] *Karlsruhe Institute of Technology, Institute for Pulsed Power and Microwave Technology, Eggenstein Leopoldshafen, 76344, Germany*
[b] *Monash University, Dept. of Chemical Engineering, Clayton Campus, Melbourne, Victoria 3800, Australia*
[c] *Parahyangan Catholic University, Dept. of Chemical Engineering, Jolan Ciumbuleuit 94, Bandung, Indonesia*
[d] *Karlsruhe Institute of Technology, Institute of Concrete Structures and Building Materials, Karlsruhe, 76131, Germany*

ABSTRACT

The use of high power microwaves to perform explosive spalling of surface concrete is a promising technique with applications in the area of concrete facilities decommissioning. The mechanism that creates explosive spalling is an interactive process of the thermal stress from high temperature gradients and the pore pressure generated from the water vaporization. In order to better predict the total stress distribution, the temperature has to be calculated by including the effect of water vaporization and water transport through a porous medium. In this paper, a one dimensional model solving the heat and diffusion equation for liquid and vapor phase with COMSOL finite element software is presented. The modelling of the drying process is based on the Spatial Reaction Engineering Approach (SREA developed by X.D. Chen). This paper discusses the influence of the relative energy activation parameter and effective diffusion coefficients on the temperature, water content and pore pressure in the case of fast microwave heating of concrete. This model is then used for a 3-D geometry with a sealed insulated concrete block and a conical antenna to compute the thermal stress, pore pressure and total stress.

Keywords: *Concrete ablation, microwave heating, drying, SREA, thermal stress, pore pressure*

1. INTRODUCTION

In the case of rapid heating of concrete with high power microwaves, evaporation/condensation of water occurs inside the porous material and leads to high thermal stress and pore pressure. The explosive spalling mechanism is not modelled in itself, but the effect of temperature and liquid content on the thermal stress and pore pressure respectively is investigated with a coupled thermo mechanical model. To better predict the temperature field for the calculation of the thermal stress (Lepers *et al.*, 2013) and the pore pressure, a porous model with solid, liquid and gas phase is currently developed. The concrete pore pressure has been calculated by different authors using coupled heat transfer models with Lamberts's law for the microwave power distribution and an equation of state based on water content for the pore pressure (Bazant and Thonguthai, 1978; Akbarnezhad and Ong, 2011).

The pore pressure was measured by Phan (2008) with explosive spalling occuring around 2.1 MPa at 240 $^{\circ}C$. In reactive powder concrete (RPC), the measured peak pore pressure was about 3.3 MPa at a temperature of 350 $^{\circ}C$ (Ju *et al.*, 2013). Bazant and Goangseup (2003b) have calculated the pore pressure with a hydro thermo mechanical model for different microwave frequencies. At 2.45 GHz and temperature in the range of $140-180\,^{\circ}C$, the pore pressure was in the range $0.3-0.8$ MPa. At 10.6 GHz and temperatures $200-350\,^{\circ}C$, the pore pressure was in the range $1-3$ MPa. They have suggested that the pore pressure could possibly trigger the mechanism of explosive spalling. In the case of concrete exposed to high temperature (such as fire for example) for time scales up to 500 min, Mindeguia *et al.* (2010) have measured the pore pressure for concrete of different compactness and showed that the low permeability concrete leads to higher pore pressure. Gawin *et al.* (2011a,b) have developed a complex multiphysics model with many parameters taking into account the moisture transport, heat transfer, thermo chemical degradation and mechanical damage. For the case of concrete heated by fire, at a time scale up to 7 h, the maximum calculated pore pressure was in the order of 0.5 MPa.

The motivation of this work is to compare the magnitude of the pore pressure with the thermal stress. With a coupled electro thermo elastic model, it is possible to see the effect of the diffusivity on the temperature distribution, moisture content, pore pressure and total stress. The Spatial Reaction Engineering Approach (SREA) developed by Chen (2008) is used to model drying processes of materials. The method was successful in predicting liquid content and spatial temperature distributions for many different porous materials such as vegetables or fruits for conventional drying (Chen and Putranto, 2013b) or wood material for example (Putranto and Chen, 2013b). The local evaporation/condensation term is proportional to the difference between the internal saturated (or equilibrium) vapour concentration and the actual water vapour concentration. The internal vapour concentration is modelled with an Arrhenius type law with a relative activation energy function to be determined experimentally by

* *Corresponding author. Email: benjamin.lepers@kit.edu*

Global Digital Central
ISSN: 2151-8629

measuring the water loss rate profile versus time. To simplify our model, the local liquid and vapor concentration are calculated with the assumption of a closed pore volume system and an ideal gas law for the behaviour of the vapour and air phase. For the 3-D coupled electromagnetic model, the complex permittivity of concrete and the thermal properties are expressed as a function of the solid, liquid and gas phase. The computation of the temperature, liquid and water vapour concentration is necessary for the calculation of the total pressure. The pore pressure is combined with a thermoelastic model to compute the total stress. In the next section, the electromagnetic model of a conical antenna based on a standard WR 340 rectangular wave guide is briefly described. Then, the heat and mass transfer model together with the mechanical model used to compute the thermal stress and pore pressure of concrete are presented. The novelty of this work is the use the SREA approach (Chen and Putranto, 2013a) in order to compute the liquid and vapor content distribution in concrete during microwave heating.

2. MATHEMATICAL MODELLING

2.1. Microwave model

The microwave power density is obtained by solving the wave equation in the frequency domain at 2.45 GHz of a 3-D conical antenna including an air gap of 10 mm between the guide aperture and the concrete surface. The power density distribution is shown in Fig. 1. The conical antenna is based on a standard 86.6×43.3 mm rectangular wave guide. The length of the conical section is 68 mm and is fully filled with Teflon PTFE. The width, heights of the entry and exit of the conical section are respectively $\{54, 43.3, 21.6\}$ mm.

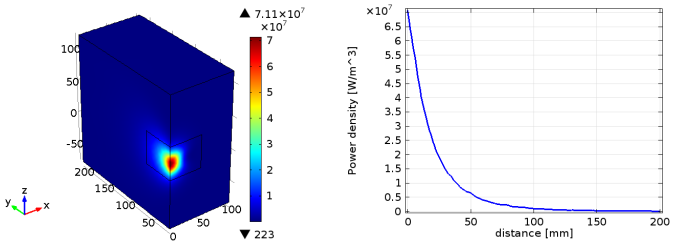

(a) (b)

Fig. 1 Power density distribution [$\mathrm{W/m^3}$] for the conical antenna with input power $P_{in} = 10$ kW and an air gap of 1 cm between the antenna aperture and the concrete bloc with a constant relative permittivity $\epsilon = 6 - 0.68j$ (a). Power density in the center along the central y axis (b).

A 1-D model allows the calculation of the temperature, water and vapour content along the thickness of the concrete wall by the solving the coupled heat and diffusion equations with much shorter computation time than a 3-D model. Following Lambert's law, an exponential decay of the E field and power density through the thickness of the concrete sample is used. The attenuation constant is obtained from the power density calculated with a 3-D conical antenna electromagnetic model as shown in Fig. 1(b) . For, $\epsilon_r = 6 - 0.68j$ at the frequency $f = 2.45$ GHz, the skin depth for the electric field is about $\delta = 4.18$ cm ($e^{-1} \simeq 0.36$ attenuation of the maximum electric field). The attenuation constant is $\beta = \frac{1}{\delta} = 23.9$ $1/\mathrm{m}$. The power density distribution used in the 1d model is:

$$q(y) = q_0 e^{-2\beta y} \tag{1}$$

with $q_0 = 70$ $\mathrm{MW/m^3}$ obtained with the 3-D conical antenna model with 10 kW of input power.

2.2. Heat and mass transfer model

2.2.1. Definitions For a solid material such as concrete, the volume variation of the concrete sample (shrinkage or expansion) during heating is negligible and the system is assumed to be a sealed domain of constant volume V and constant porosity.

$$V = V_s + V_l + V_v + V_a \tag{2}$$

The subscript s, l, v, a designating the solid, liquid, vapour and air phase. The porosity ϵ_0 and the solid fraction are:

$$\epsilon_0 = \frac{V_l + V_v + V_a}{V} \qquad 1 - \epsilon_0 = \frac{V_s}{V} \tag{3}$$

The solid C_s and local liquid C_l, vapor concentration C_v and air concentration C_a in $\mathrm{kg/m^3}$ are:

$$\begin{aligned} C_s &= \frac{m_s}{V} = \frac{m_s}{V_s}\frac{V_s}{V} = \rho_s\,(1-\epsilon_0) \\ C_l &= \frac{m_l}{V} = \frac{m_l}{m_s}\frac{m_s}{V} = X_l C_s = \rho_l f_l \\ C_v &= X_v C_s = \rho_v f_v \\ C_a &= X_a C_s = \rho_a f_a \end{aligned} \tag{4}$$

X_l, X_v and X_a are the local mass of liquid, vapour and air per kg of dry solid and $f_i = \frac{V_i}{V}$, $i = \{l, v, a\}$ are respectively the volume fraction of liquid, vapour and air. For a closed volume, the air concentration is constant since the mass of air is constant.

2.2.2. Assumptions The assumptions used for the heat and mass transfer processes inside the porous model of concrete are:

- The effect of solid shrinkage or expansion on heat and mass transfer process is not taken into account, a sealed and constant volume is assumed.
- cracks formation and sudden increase of permeability are not modelled.
- The porous medium is homogeneous and isotropic (i.e. k, D_l, D_v are scalar quantities).
- The diffusion coefficients are assumed to be constant. In reality, they are usually function of temperature and water content.
- The transfer of liquid and vapour water occurs by diffusion, the "effective diffusion " coefficient includes all the contribution to the fluid movement such as temperature and pressure gradient (Chen, 2007).
- The evaporation/condensation rate is proportional to the difference between the internal saturated vapour concentration $C_{int,sat}$ and the current concentration inside the solid C_v.
- Because of fast microwave heating and for simplification of the analysis, the volume is sealed and insulated, no heat flux and mass flow (water or gas) cross its boundaries. In total, all the boundaries condition on the surface of the bloc are: $\mathbf{n}.\nabla T = 0$, $\mathbf{n}.\nabla C_l = 0$, $\mathbf{n}.\nabla C_v = 0$ with $\mathbf{n}$ the unit vector normal to the surface.
- The initial temperature and moisture content are uniformly distributed.
- The water vapour and air phase follow the ideal gas law.

Global Digital Central
ISSN: 2151-8629

2.2.3. Heat and mass transfer equations The temperature field is calculated with the heat equation for a porous medium

$$\rho c_p \frac{\partial T}{\partial t} = \nabla \cdot k \nabla T + q_{em} - I \Delta H \tag{5}$$

with the thermal properties averaged with the solid, water and gas content (see appendix A). q_{em} is the power density source term from microwave heating and I the rate of evaporation/condensation. $\Delta H = 2257$ kJ/kg is the latent heat of vaporization of liquid water and assumed to be constant in the range $20 - 300\,^{\circ}C$ independent of the temperature (in reality, $\Delta H = \Delta H(P,T)$). The initial temperature of the concrete block in the model is $T_i = 20\,^{\circ}C$. The spatial distribution of the liquid and vapour concentration at different times are calculated with the diffusion equations:

$$\begin{aligned} \frac{\partial C_l}{\partial t} &= \nabla \cdot D_l \nabla C_l - I \\ \frac{\partial C_v}{\partial t} &= \nabla \cdot D_v \nabla C_v + I \\ I &= h_{m,in} A_{in} (C_{int,sat} - C_v) \end{aligned} \tag{6}$$

D_l and D_v are the effective diffusivity of the liquid and vapour phase and depends of the micro structure of the porous material, the temperature and pressure gradient (Chen, 2007). The effective diffusivity can be function of the temperature and water content (Zhang and Datta, 2004). It is assumed to be constant in this paper to facilitate the interpretation of the solution of the coupled heat and mass transfer equations. The heat Eq. (5) for temperature and the diffusion Eqs. (6) for liquid and vapour concentrations are coupled with the source/depletion term I modelling the evaporation/condensation process. This term is explained in more details in the subsection 2.2.4 with the description of the drying model. The concept of using the reaction engineering approach to model this evaporation/condensation term is based on the fact that this process can be seen as an activation process. $h_{m,in}\,[\mathrm{m/s}]$ is the internal mass transfer coefficient associated with the pore surfaces (Chen and Putranto, 2013a). $A_{in}\,[\mathrm{m^2/m^3}]$ is the internal surface area per cubic meter. It depends on the micro structure of the porous material (Putranto and Chen, 2013a). The product $h_{m,in}A_{in}$ depends on the micro structure of the porous media.

2.2.4. Drying model The drying model is based on the evaporation (or condensation) term proportional to the difference between the equilibrium vapour pressure (or concentration) and the actual vapour pressure. $I \propto (P_{v,sat} - P_v) \propto (C_{v,sat} - C_v)$. The equilibrium vapour pressure and concentration are commonly called the saturated vapour pressure $P_{v,sat}$ and concentration respectively $C_{v,sat}$. To understand this relation a constant volume with a mixture of water and vapour with three different states is considered:

Equilibrium, state 1
The closed system is in equilibrium with the environment, in this case the partial pressure of vapour is the equilibrium vapour pressure, $P_{v1} = P_{v1,sat}$ equivalent to $C_{v1} = C_{v1,sat}$. The number of gas molecules entering to the liquid equals the number of molecules leaving the liquid and entering into the gas phase . Macroscopically, there is no evaporation or condensation $I = 0$.

Heating, state 2
The system is suddenly heated, the temperature and total pressure increase. In this case the saturated vapour pressure reaches a new state $P_{v2,sat} > P_{v1,sat}$. The vapour pressure P_v of the mixture will increase until $P_{v2,sat}$ to reach this new equilibrium. During this process, $I > 0$ and evaporation occurs.

Cooling, state 3
The system is initially in state 1 and then suddenly cooled. In this case, the saturated vapour pressure drops to reach a new state $P_{v3,sat} < P_{v1,sat}$. The vapour pressure P_v of the mixture will decrease until $P_{v3,sat}$. During this transformation, $I < 0$ and condensation occurs. In this description of heating and cooling transformations of the liquid vapour mixture, the saturated (or equilibrium) vapour pressure and partial vapour pressure can be interchanged by the saturated vapour concentration and vapour concentration.

The SREA approach to model the drying of a porous medium considers that additional energy is required to evaporate the liquid inside the solid (compared to free space for example). The evaporation/condensation term is modified and proportional to the difference between the internal saturated vapour concentration $C_{int,sat}$ and the actual vapour concentration C_v. In summary, when the vapour concentration of the actual state is lower (higher) than the internal saturated vapour concentration, vapour is produced (consumed) with $I\Delta H$ being the power per unit volume absorbed during evaporation and released during condensation. For $C_{v,s} = C_v$, $I = 0$, the internal vapour concentration equals the vapour concentration, there is no evaporation or condensation and the system is in equilibrium. The main idea to model the drying process with the SREA approach is to consider evaporation as an activation process that can be described by an Arrhenius equation (Chen and Putranto, 2013a):

$$C_{int,sat} = \exp\left(-\frac{\Delta E_v}{RT}\right) C_{v,sat} \tag{7}$$

This Eq. (7) shows that if the activation energy ΔE_v is 0, then the internal saturated concentration is the saturated concentration in free space. If the ΔE_v takes large values, then $C_{int,sat} << C_{v,sat}$ and evaporation will be small. The saturated vapour concentration $C_{v,sat}$ is not the same as the saturated partial vapour density of water $\rho_{v,sat}$ but can be linked to it by taking into account the porosity and the actual liquid concentration C_l:

$$\begin{aligned} C_{v,sat} &= \rho_{v,sat} \frac{V_g}{V} \\ &= \rho_{v,sat} (\epsilon_0 - \frac{V_l}{V}) \\ &= \rho_{v,sat} (\epsilon_0 - \frac{C_l}{\rho_l}) \end{aligned} \tag{8}$$

With $V_g = V_v + V_a$ the volume of the gas phase. $\rho_{v,sat}$ is the partial density of the saturated vapour defined in respect to the gas volume and expressed with the Clapeyron relation (22) from appendix A. The partial density of air and vapour are function of the temperature and pressure described with the ideal gas law. ΔE_v is the apparent activation energy and can be expressed with a relative energy function:

$$\begin{aligned} \Delta E_v &= f(X_l, X_{l0}, X_\infty) \Delta E_\infty \\ \Delta E_\infty &= -RT_\infty ln(RH_\infty) \end{aligned} \tag{9}$$

ΔE_∞ represents the equilibrium activation energy or the activation energy of the dry state. $X_l = \frac{C_l}{C_s}$, is the actual water content per unit mass of dry solid. X_{l0}, X_∞ are given and are the liquid content of the initial and final states respectively. RH_∞ and T_∞ are the relative humidity and temperature of the dry state. To model a drying behaviour of a particular porous sample the relative activation energy could be of the form for example:

$$\begin{aligned} f(X_l) &= \left(\frac{X_{l0} - X_l}{X_{l0} - X_{l\infty}}\right)^n \\ f(X_{l0}) &= 0 \\ f(X_{l\infty}) &= 1 \end{aligned} \tag{10}$$

Global Digital Central
ISSN: 2151-8629

In principle, it should be obtained from a drying experiment but as explained in this section below, it was not possible to experimentally obtain this function. The activation energy expressed in Eq. (9) will be used in the heat and diffusion Eqs. (5) and (6). Using Eq. (7), the internal saturated vapour concentration can be expressed as:

$$C_{int,sat}\left(X_l,T\right)=RH_{\infty}^{\frac{T_{\infty}}{T}\left(\frac{X_{l0}-X_l}{X_{l0}-X_{l\infty}}\right)^n}C_{v,sat}\left(T\right) \tag{11}$$

in particular:

$$\begin{aligned} C_{int,sat}\left(X_{l\infty},T\right) &= \left(RH_{\infty}\right)^{\frac{T_{\infty}}{T}}C_{v,sat}\left(T\right) \\ C_{int,sat}\left(X_{l\infty},T_{\infty}\right) &= \left(RH_{\infty}\right)C_{v,sat}\left(T_{\infty}\right) \\ C_{int,sat}\left(X_{l0},T\right) &= RH_{\infty}^{0}C_{v,sat}(T)=C_{v,sat}(T) \end{aligned} \tag{12}$$

The Eq. (12) gives the definition of the relative humidity of the drying medium, i.e. the ratio between the vapour concentration and saturated vapour concentration of the dry state. The last equation shows that for the particular initial wet state with water concentration X_{l0}, the internal vapour concentration equals the saturated water vapour concentration in free space. For an accurate drying model of the system, the relative activation energy should be obtained from measurements. The time duration to achieve explosive spalling under high power microwave is in the order of $10\,s$. This short time scale gives some experimental difficulties for the measurement of the weight loss of water content during microwave heating. In this sense, it is not a classical drying problem. In operation, the antenna and concrete block are placed in a shield metallic box to avoid any microwave leakage and the high electric field in the vicinity of the concrete sample does not allow to place sensitive electrical equipment nearby. According to the spatial engineering approach, the measurement of the water loss rate versus time is the central point to extract the relative activation energy function. This process will capture the behaviour of the porous material under drying conditions. In the case of rapid heating with high power microwaves, the rate of water content loss versus time was not available and the relative activation energy could not be built. For this reason, it was decided to perform the simulations for the two extreme cases of the relative activation energy function $f=0$ and $f=1$ over the whole range, from wet to dry state $X_{l\infty}<X_l<X_{l0}$.

Maximum evaporation ($f=0$)
In this case, the activation energy is $f=0$, $C_{int,sat}=C_{v,sat}$ and $I=hA\left(C_{v,sat}-C_v\right)$.

Maximum restricted evaporation ($f=1$)
For the case of maximum restricted evaporation, $f=1$, $C_{int,sat}=RH_{\infty}^{\frac{T_{\infty}}{T}}C_{v,sat}$ and $I=h_{min}A_{in}(RH_{\infty}^{\frac{T_{\infty}}{T}}C_{v,sat}-C_v)\simeq 0$.

2.3. Mechanical model

With a 3-D mechanical model, it is possible to calculate the thermal stress from the temperature field. The total stress is calculated by adding the internal stress from the pore pressure on the diagonal components of the stress tensor.

2.3.1. Solid equilibrium

$$\rho\ddot{\mathbf{u}}(\mathbf{x},t)-\nabla\cdot\boldsymbol{\sigma}(\mathbf{x},\boldsymbol{t})-\boldsymbol{\kappa}(\mathbf{x},t)=0 \tag{13}$$

The mechanical model is based on force equilibrium (or Newton law extended to solids) with ρ the density of the solid, $\mathbf{u}$ the displacement vector, $\boldsymbol{\sigma}$ is the material stress tensor for small deformation. $\boldsymbol{\kappa}$ is the external volume forces such as gravity or magnetic forces. In our case, gravity can be neglected in comparison to internal thermal stress. In addition, the inertial term $\rho\ddot{\mathbf{u}}$ was neglected in comparison to the thermal stress because the time of the duration of the "heat pulse" (microwave heating about 10 s) is much larger than the characteristic time of propagation of stress waves inside the solid (speed of sound in the material over a characteristic length of the solid). The Eq. (13) without the inertial term is also called the quasi static approximation equilibrium of solids.

2.3.2. Linear elastic constitutive law

The constitutive law used to model the concrete material behaviour is a linear elastic model or generalised 3d Hooke's law as shown in Eq. (14). This behaviour is realistic in the elastic regime of the material. Three parameters are used to define the relationship between the strain $\boldsymbol{\epsilon}$ and the stress $\boldsymbol{\sigma}$ in the case of thermal expansion with a temperature difference ΔT. The young module E, which represents the stiffness of the material, the poisson ratio ν which is the ratio between longitudinal and lateral displacement, and the linear thermal expansion coefficient α. The pressure p is obtained from the heat diffusion model calculating the temperature, water and vapour content distribution inside the solid.

$$\begin{aligned} \boldsymbol{\sigma} &= \boldsymbol{\sigma}_0+\frac{E}{1+\nu}\boldsymbol{\epsilon}+\frac{E\nu}{(1+\nu)(1-2\nu)}tr(\boldsymbol{\epsilon})\mathbf{I}-\alpha\frac{E}{1-2\nu}\Delta T\mathbf{I} \\ \boldsymbol{\sigma}_0 &= -p\boldsymbol{I} \end{aligned} \tag{14}$$

The effect of the pore pressure p is implemented as an initial stress $\boldsymbol{\sigma}_0$ operating only the diagonal components of the stress tensor $\boldsymbol{\sigma}$. The Von Mises stress $\sigma_m=\frac{1}{\sqrt{2}}\sqrt{(\sigma_1-\sigma_2)^2+(\sigma_2-\sigma_2)^2+(\sigma_3-\sigma_1)^2}$, is used to evaluate the stress state inside the solid and to compare with the maximal material strength. σ_i are the main stress components of the stress tensor. For concrete material, the maximum tensile or compressive strength depends on the loading scenario and more realistic failure criterion as the Von Mises stress have been developed. The choice of the failure criterion for concrete material is a field of research and is not discussed in the present paper.

2.3.3. Boundary conditions

On all faces of the cube and the symmetry plane only tangential displacements are allowed, i.e $\mathbf{n}\cdot\mathbf{u}=0$ with $\mathbf{n}$ the vector normal to the corresponding face. The face in front the aperture of the wave guide is not constrained, the displacements are allowed in all directions.

3. IMPLEMENTATION

3.1. 1-D model

The coupling term I between the heat and diffusion equations is modelled with the reaction engineering approach. Using Eqs. (7) and (8), it is written:

$$I=h_{m,in}A_{in}\left[\exp\left(\frac{-\Delta E_v}{RT}\right)\rho_{sat}\left(\epsilon_0-\frac{C_l}{\rho_l}\right)-C_v\right] \tag{15}$$

with ρ_{sat} given in from appendix A. The heat transfer, and partial differential equations node are chosen to solve the heat and diffusion Eqs. (6) with COMSOL 4.4 multiphysics software. The resolution of these partial differential equations is performed with the finite element method and adequate numerical methods incorporated in the software. The calculated fields are the temperature T, the liquid concentration C_l and the vapor content C_v. The liquid and vapor content X_l and X_v are calculated from Eq. (4). With the assumption of a constant sealed pore volume $V_{gas}=(\epsilon_0-\frac{C_l}{\rho_l})V$, the total pore pressure is calculated with the partial pressure of vapour and air:

$$\begin{aligned} p_v &= \frac{RT}{M_v}\frac{m_v}{V_{gas}}=\frac{RT}{M_v}\frac{C_v}{(\epsilon_0-\frac{C_l}{\rho_l})} \\ p_a &= \frac{RT}{M_a}\frac{m_a}{V_{gas}}=\frac{RT}{M_a}\frac{C_a}{(\epsilon_0-\frac{C_l}{\rho_l})} \\ p &= p_v+p_a \end{aligned} \tag{16}$$

with $R=8.3\ \mathrm{J/(mol.K)}$, the universal gas constant and $\{M_v,M_a\}=\{18,29\}\ \mathrm{g/mol}$ the molar mass of the vapour and air. ϵ_0 is the porosity previously defined in subsection 2.2.1 and used to define the volume occupied by the liquid and gas phase. The simulation was focused on the influence of the activation energy and the diffusion coefficient. Because the relative activation energy function of concrete is not known, the

Global Digital Central
ISSN: 2151-8629

two extreme values 0 (evaporation) and 1 (no evaporation) are used. The diffusion coefficients for vapour chosen for the simulation are: $D_v = \{10^{-2}, 10^{-4}, 10^{-9}\}$ m^2/s. The initial water content used for the model is $X_{l0} = 0.05$ kg/kg dry solid.

3.2. 3-D model

The 3-D model solves the wave equation in the frequency domain, the heat and diffusion equations and the thermo elastic equations are solved every 2 s until 10 s. It is a non linear problem because the dielectric permittivity is function of the water content and needs to be updated at each time step. After solving this first problem, the temperature field and pore pressure are available and a second study is used to solve the mechanical model.

4. SIMULATION RESULTS AND DISCUSSION

4.1. Analytic estimation

4.1.1. Temperature increase For the maximum power density of $q = 70$ MW/m^3 with $\Delta t = 10$ s of heating, with constant thermal properties and an adiabatic system, the temperature increase can be estimated from energy conservation during this amount of time:

$$\begin{aligned} \Delta T &= \frac{q\Delta t}{\rho c_p} \\ &\simeq 364\,^\circ C \end{aligned} \tag{17}$$

with $\rho = 2400$ kg/m^3 and $c_p = 800$ J/(kg.K).

4.1.2. Thermal stress In the case of a 1d geometry and assuming a linear elastic behaviour with Hooke's law, the thermal stress is related to the thermal strain:

$$\sigma = E\epsilon = E\alpha\Delta T \tag{18}$$

with $E = 30\,GPa$ and $\Delta T = 300\,^\circ C$, if we assume that for fast heating the concrete solid is blocked, the order of magnitude for the stress is $\sigma \simeq 90\,MPa$ which exceeds the tensile strength of most concrete. This estimation gives an upper limit of the possible stress because it is based on the maximal temperature difference possible and because the solid is completely blocked.

4.1.3. Pore pressure Water can be in liquid or gas state depending on the pressure and temperature conditions. In a pressure-specific volume (P-v) or pressure-temperature (P-T) diagram of water, the curves delimiting the different states of water are called the saturated curves. For a pure substance in a closed volume, the saturated vapour pressure, is the pressure of the gas phase when in equilibrium with the liquid phase. The pressure evolution of a water vapour mixture is calculated for a constant volume (isochoric transformation) from an initial state of $T = 100°C$ and $P = 101.3$ kPa to the final state with temperature $T = \{200, 300\}°C$ in order to estimate the maximal possible pore pressure. The initial specific volume for this initial state of the saturated liquid water and vapour are $v_{vs1} = 1.67\,m^3/kg$, $v_{ls1} = 1.044\,dm^3/kg$. For the final states at $T = \{200, 300\}\,^\circ$C the specific volume of liquid and vapour are respectively $\{v_{ls200}, v_{ls300}\} = \{1.156, 1.404\}\,dm^3/kg$ and $\{v_{vs200}, v_{vs300}\} = \{127.36, 21.67\}\,dm^3/kg$. If we have an initial state made of a mixture of water and vapour, the mean specific volume of the mixture liquid and vapour is defined as:

$$\bar{v} = v_l + (v_v - v_l) \times x \tag{19}$$

with v_l, v_v the specific volume of the liquid and vapour phase. $x = \frac{m_v}{m}$ is called the quality factor of the liquid - vapor mixture, m_v and m are the mass of the vapour and the total mass of the fluid respectively. The final pressure is calculated for the liquid vapour mixture of different initial quality factor $x = \{0.01, 0.1, 0.4, 1\}$. In the table 1, the pressure of the water and vapour mixture is calculated for different quality factor

x	0.01	0.1	0.4	1
$\bar{v}$ $[m^3/kg]$	0.0178	0.1682	0.6698	1.6729
P_{200} [MPa]	1.553	1.208	0.325	0.130
P_{300} [MPa]	8.581	1.519	0.397	0.157

Table 1 Pressure of the liquid-vapour mixture for an isochoric transformation from initial state $T = 100\,^\circ$C and atmospheric pressure to the final temperatures $T = \{200, 300\}\,^\circ$C

and for the two final temperatures $T = \{200, 300\}\,^\circ$C for the isochoric transformation (specific volume is constant from state 1 to state 2 , $\bar{v}_2 = \bar{v}_1$).

From table 1, the specific volume of the mixture with $x = 0.01$ is $\bar{v} = 17.8$ dm^3/kg and bounded by saturated liquid and vapour specific volume $\{v_{ls200}, v_{ls300}\} < \bar{v} < \{v_{vs200}, v_{vs300}\}$ for the final state at $\{200, 300\}\,^\circ$C. In this case, the corresponding state is a mixture of liquid and vapour and the corresponding pressure is the saturated vapour pressure at these corresponding temperature, $T = \{200, 300\}\,^\circ$C. For the mixtures with higher vapour quality factor $x = \{0.1, 0.4, 1\}$, their specific volume are higher than the specific volume of the saturated vapour $\bar{v} = \{v_{x0.1}, v_{x0.4}, x_{x1}\} > \{v_{vs200}, v_{vs300}\}$, these mixtures are in the super heated vapour state. Looking into the corresponding table for super heated vapour and for the specific volume, the pressure can be obtained. For the same temperature increase, a high vapour mixture tends to give a smaller pressure than a high liquid mixture. The mixture with high vapour content behaves more closely to a perfect gas. The pressure ranges from 1.5 MPa for a mixture with $x = 0.01$ content to 0.13 MPa for pure vapour ($x = 1$) at $T = 200\,^\circ$C. The pressure ranges from 8.6 MPa for a mixture with $x = 0.01$ to 0.16 MPa for pure vapour at $T = 300\,^\circ$C.

The saturated (or equilibrium) vapour pressure of pure water can also be calculated with the Clapeyron equation:

$$\ln \frac{p_{sat}(T)}{p_0} = \frac{H}{R}\left(\frac{1}{T_0} - \frac{1}{T}\right) \tag{20}$$

if we assume that the latent heat of vaporisation of water is constant $H = 40$ kJ/mol. $R = 8.3$ J/(mol.K) is the universal gas constant. $T_0 = 373$ K with the corresponding saturated vapour pressure $p_0 = 101.3$ kPa can be chosen for example. For the case of very fast heating, an isochoric transformation is a logic assumption, since water does not have time to move through the porous medium. In reality the time scale of the mass transfer is larger or the same order than the time scale of heat transfer through the porous medium and so the transformation of the water vapour mixture during microwave heating is not isochoric. The volume of the mixture water and vapour may increase during heating, (for example if steam is moving through a open pore networks) causing a reduction of the pressure. Hence, the isochoric transformation assumption gives an upper limit of the pore pressure during fast heating. If the liquid-vapour mixture is mixed with air, the total pressure will be the sum of the partial pressure of the vapour and the air.

4.1.4. Time scale analysis With a characteristic length L of the micro structure of the medium and the thermal properties of the solid phase of the concrete taken from appendix A, $\kappa = \frac{k}{\rho c_p} \simeq 8.8 \times 10^{-7}$ m^2/s the thermal diffusivity of dry concrete, and D the mass diffusion coefficient, the time scales for the heat and mass diffusion are:

$$\begin{aligned} t_{heat} &= \frac{L^2}{\kappa} \\ t_{diff} &= \frac{L^2}{D} \\ \frac{t_{heat}}{t_{diff}} &= \frac{D}{\kappa} \\ D &= \frac{t_{heat}}{t_{diff}}\kappa \end{aligned} \tag{21}$$

Frontiers in Heat and Mass Transfer (FHMT), 5, 13 (2014)
DOI: 10.5098/hmt.5.13

Global Digital Central
ISSN: 2151-8629

If the porous medium has large open porosity or cracks, the time constant for the mass diffusion mechanism can be smaller than the thermal time constant. In this case, the diffusion coefficient can be much larger than the thermal diffusivity. On the contrary, for a sealed domain with closed porosity, there is no mass diffusion possible, $t_{diff} = \infty$ and the diffusion coefficient D is 0. In our first simulation, it was assumed that $D_l \simeq 0 << D_v$. The vapour diffusion coefficient is assumed to be constant (not the case in reality) and simulations were made for a large and a small vapour diffusion $D_v = \{10^{-2}, 10^{-9}\}$ m^2/s coefficient.

4.2. Numerical results

4.2.1. 1-D model In this section, the power density, temperature, liquid content, vapour content and pore pressure distribution through the first 10 cm thickness of the 40 cm sample are given for the extreme values of the relative activation energy corresponding to maximum evaporation ($f = 0$) and no evaporation ($f = 1$). The simulation are made for three different values of vapour diffusion coefficients $D_v = 10^{-2}, 10^{-4}, 10^{-9}$ m^2/s. All these calculated variables are represented along the depth of the concrete and after 10 s of microwave heating with 10 kW input power. A large vapour diffusion coefficient was chosen to evaluate the effect of diffusion on the time scale of 10 s. This could hypothetically correspond for example to an open cracks where a large passage through the porous medium is available for vapour transport.

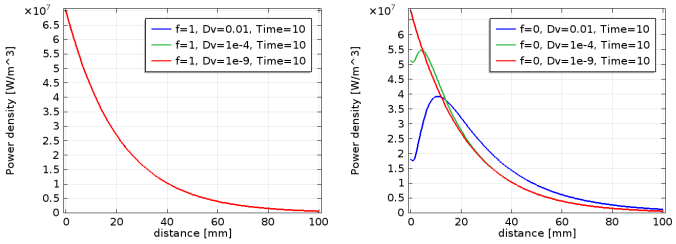

(a) $f = 1$ (b) $f = 0$

Fig. 2 Power density [W/m^3] for $D_v = \{10^{-2}, 10^{-4}, 10^{-9}\}$ m^2/s with no evaporation (a) and with evaporation (b)

Power density In case of no evaporation ($f = 1$), the Fig. 2(a) shows that the power density distribution is independent of the vapour diffusion coefficient. Because there is no evaporation process inside the material, no vapour is created and the local liquid and vapour content remains constant. For this reason, the power density profile is not modified by different diffusion coefficients. The Fig. 2(b) with maximum evaporation $f = 0$ shows that the power density is modified from the endothermic evaporation process. With larger vapour diffusion coefficient, vapour is transported through the material and more evaporation occurs. When the temperature of the water vapour mixture decreases in contact of the colder domains of the solid skeleton of the porous medium, the temperature can be lower than the saturation temperature of the mixture. In this case, condensation occurs and the vapour releases latent heat during the condensation process. The Fig. 2(b) shows that for depth above 1 cm the power density magnitude for $D_v = 0.01$ m^2/s case (blue curve) is higher than the case with limited vapour transport ($D_v = 10^{-9}$ m^2/s, red curve). In this case, heat from condensation has been released to the concrete in the colder part of the domain. It is also interesting to see that the maximum of the power density is located at $y \simeq \{4, 10\}$ mm for $D_v = \{10^{-4}, 10^{-2}\}$ m^2/s respectively.

Temperature The Fig. 3(a) shows that there is no influence of the vapor diffusivity because there is no evaporation. The power density is unchanged and so the thermal properties. The Fig. 3(b) shows the effect

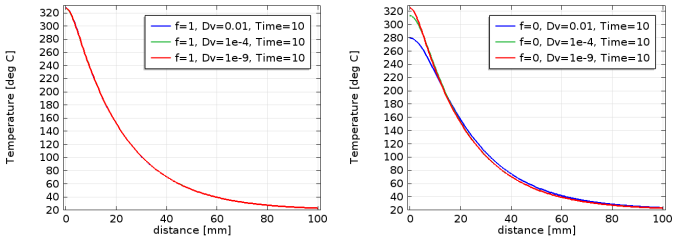

(a) $f = 1$ (b) $f = 0$

Fig. 3 Temperature [°C] for $D_v = \{10^{-2}, 10^{-4}, 10^{-9}\}$ m^2/s with no evaporation (a) and with evaporation (b)

of evaporation and vapour transport on the surface with a temperature difference of about 40 °C between limited (red curve) and large vapour transport (blue curve). A maximum surface temperature around 300 °C is realistic and was observed experimentally in our laboratory (See thermo camera picture in appendix B).

Liquid and vapor content Figures 4(a) and 4(b) show the liquid and vapor content for the case of maximum evaporation and for the 3 diffusion coefficients. The case of no evaporation is not of interest because the liquid and vapour content remain unchanged. More liquid is removed in the first 1 cm concrete depth when the vapour diffusivity increases. For the $D_v = 10^{-9}$ m^2/s the vapour increases locally near the surface. For $D_v = 10^{-2}$ m^2/s, the vapour diffuses through the thickness. It is also interesting to observe that locally the water content X_l can exceed the uniform initial water content X_{l0}. This is due to the transport and condensation of steam. These different vapour distribution through the thickness explains the different vapour and pore pressure distribution inside the sample.

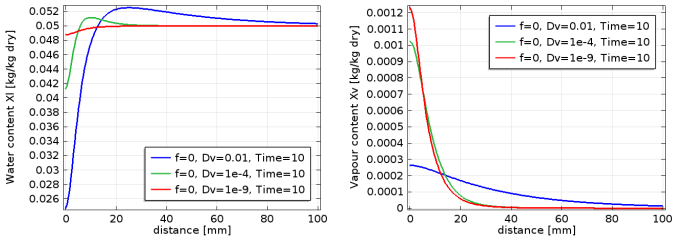

(a) X_l (b) X_v

Fig. 4 Liquid content X_l [−] (a) and vapor content X_v [−] (b) for $D_v = \{10^{-2}, 10^{-4}, 10^{-9}\}$ m^2/s

Total pressure The Fig. 5(a) shows that the peak pressure near the surface is about 0.2 MPa. For a sealed volume, with no vapour creation from the liquid phase, the effect of pressure build up with temperature is mostly due to the thermal expansion of air and vapour, according to the ideal gas model, the pressure is proportional to the temperature. The Fig. 5(b) shows that the peak pressures are $P \simeq \{2, 9, 14\}$ MPa for $D_v = \{10^{-2}, 10^{-4}, 10^{-9}\}$ m^2/s respectively. Near the surface, vapour is rapidly created and moves through the solid with a velocity function of the porosity of the material (or the diffusion coefficient). The partial pressure of vapour is proportional to the vapour concentration through the ideal gas law for a given temperature. At the maximum temperature of 320 °C, the saturated vapour pressure of liquid vapour water is 11.3 MPa. For the smallest diffusion coefficient, the calculated pressure of 14 MPa slightly exceeds the saturated vapour pressure. This means

that the specific volume of the liquid vapour mixture exceeds the saturated specific volume, in this case the state of vapour is called superheated steam.

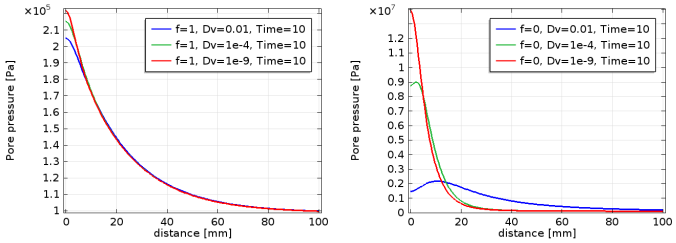

(a) $f = 1$ (b) $f = 0$

Fig. 5 Total pore pressure P [Pa] for $D_v = \{10^{-2}, 10^{-4}, 10^{-9}\}$ m^2/s with no evaporation (a) and with evaporation (b)

Materials properties The complex permittivity and thermal properties (thermal diffusivity and specific heat) expressed as a function of the solid, liquid and gas phase properties and weighted with the corresponding volume fraction (see appendix A), are plotted in Figs. 6 and 7. The value of the real part is between 6.7 and 8, the imaginary part is between 0.4 for the dry state and 0.7 for the wet state. The dielectric properties follow closely the liquid content distribution because it is the dominant factor that influence the dielectric properties for a constant temperature (At room temperature, free water has a real part of the relative permittivity of about 80, but in the case of concrete, the water is also bounded and for this reason the real part was taken to be 30). The dielectric properties are also strongly affected by temperature, but this effect is not investigated in this study.

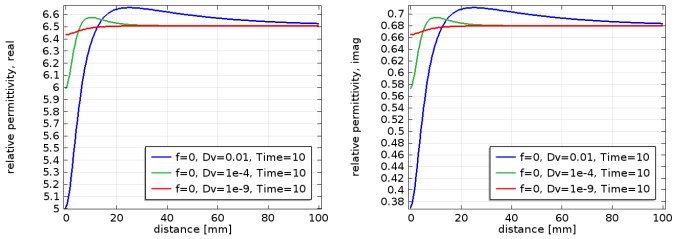

(a) ϵ^{real} (b) ϵ^{im}

Fig. 6 Relative permittivity, real part (a) and imaginary part (b) with evaporation for $D_v = \{10^{-2}, 10^{-4}, 10^{-9}\}$ m^2/s

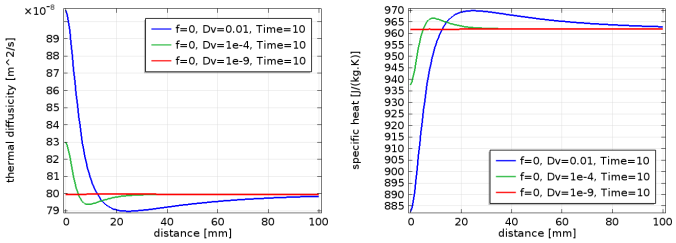

(a) κ (b) c

Fig. 7 Effective thermal diffusivity (a) and effective specific heat [J/(kg.K)] (b) with evaporation for $D_v = \{10^{-2}, 10^{-4}, 10^{-9}\}$ m^2/s

The Fig. 7(a) shows the effective thermal diffusivity for the 3 different diffusion coefficients with values between $\{79, 91\} \times 10^{-8}$ m^2/s. The Fig. 7(b) shows the effective thermal specific heat with values between $\{885, 970\}$ J/(kg.K). The effective specific heat decreases during microwave heating because of the decrease of the water content inside the first centimetre of the concrete.

4.2.2. 3-D model The 3-D model solves the wave equation in the frequency domain at 2.45 GHz. A time dependant solver is used to couple the electromagnetic model to the heat transfer and mechanical model. The complex dielectric permittivity of the concrete is expressed as a function of the solid, liquid and gas phase. The thermal properties are also depending on the liquid and gas content (see appendix A). Material properties are updated at each time steps and the electromagnetic model computed with the updated dielectric permittivity of the porous material. The mechanical model solves the elasticity equations to obtain the thermal stress from the temperature of the heat transfer model. The total stress is computed by adding the pore pressure as an initial stress contribution. The pore pressure is calculated with the distribution of the water and vapour content obtained from the coupled heat and mass transfer model. The results are presented for the case of no diffusion $D_v = 0$ m^2/s and with large diffusion $D_v = 10^{-2}$ m^2/s with $f = \{0, 1\}$.

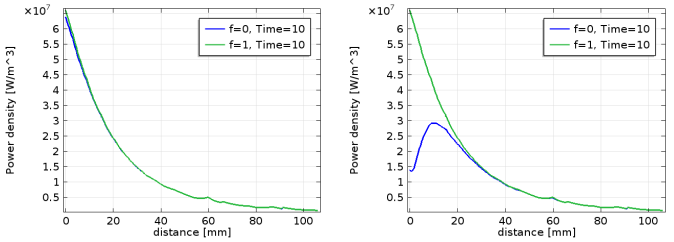

(a) (b)

Fig. 8 Power density [W/m^3] for $D_v = 0$ m^2/s (a) and $D_v = 10^{-2}$ m^2/s (b) and with evaporation (blue) and no evaporation (green)

Power density The Fig. 8(a) shows that power density for $f = 0$ and $f = 1$ is nearly identical. The Fig. 8(b) shows that in the case of evaporation, the maximum of the power density is about 30 MW/m^3 and located about 1 cm inside the material. The power profile is similar with the power profile from the 1-D model (see figure 2(b)). The discrepancies are due to some difference in the given initial power density and the variation of the dielectric permittivity with the 3 phases in the case of the 3-D model (See blue curves of Figs. 2(b) and 8(b)).

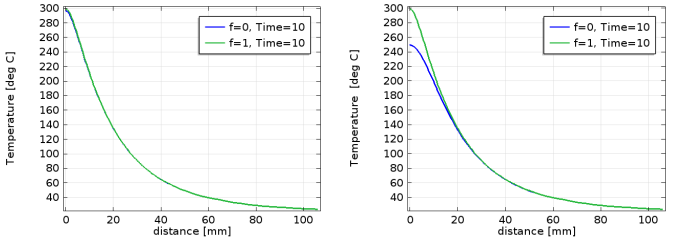

(a) (b)

Fig. 9 Temperature [°C] for $D_v = 0$ m^2/s (a) and $D_v = 10^{-2}$ m^2/s (b) and with evaporation (blue) and no evaporation (green)

Temperature The maximal temperature is about 300 °C (see figure 9(a)) near the surface for the case with no diffusion (320 °C for the 1-D case). The Fig. 9(b) shows that with high diffusion and evaporation, the maximum temperature is about 250 °C (280 °C for the 1-D case). The temperature calculated with the 1-D model are slightly higher because the microwave power density does not vary with the dielectric permittivity since the power density is approximated with Lambert's law. The comparison of Figs. 2(b) and 8(b) shows that the maximum power density with evaporation is about 40 $\mathrm{MW/m^3}$ and 30 $\mathrm{MW/m^3}$ for the 1-D and 3-D model respectively.

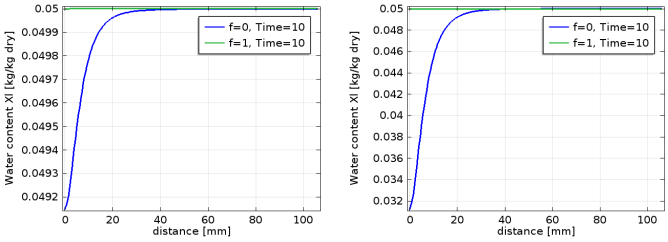

(a) (b)

Fig. 10 Liquid content X_l [−] for $D_v = 0\,\mathrm{m^2/s}$ (a) and $D_v = 10^{-2}\,\mathrm{m^2/s}$ (b) and with evaporation (blue) and no evaporation (green)

Liquid content The liquid content shown in Fig. 10 decreases near the surface of the concrete. For the case of no diffusion $X_l \simeq 0.0492$ kg/kg at the surface an about 0.032 kg/kg for the case with large diffusion and is comparable to the 1-D case with $X_l \simeq 0.026$ kg/kg from Fig. 4(a).

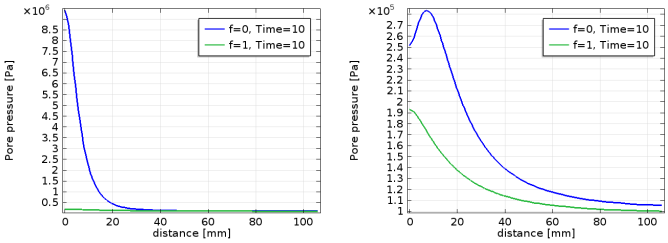

(a) (b)

Fig. 11 Pore pressure P [Pa] for $D_v = 0\,\mathrm{m^2/s}$ (a) and $D_v = 10^{-2}\,\mathrm{m^2/s}$ (b) and with evaporation (blue) and no evaporation (green)

Total pressure Figure 11(a) shows that the maximum pressure near the surface is about 9.5 MPa when evaporation occurs. At 300 °C the saturated vapour pressure of water is 8.5 MPa. With large vapour diffusivity, the Fig. 11(b) shows lower pressure with a maximum of 0.3 MPa located 7 mm in depth. The pressure profile is similar to the pore pressure profile calculated by Bazant and Goangseup (2003a,b) with a maximum of 0.2 MPa at 2.45 GHz.

Von Mises stress In the case of high diffusion, the effect of the pressure on the Von Mises stress is negligible ($\frac{\sigma}{P} \simeq 100$) and therefore not visible in Fig. 12(b). In the case of no diffusion which could correspond to a high performance concrete), the difference in the Von Mises stress when the effect of the total pressure is included or not is about 8 MPa (see Fig. 12(a)). The total stress is mostly driven by the thermal stress function of the temperature gradients.

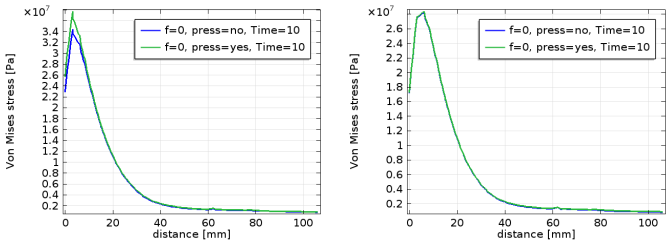

(a) (b)

Fig. 12 Von Mises [Pa] for $D_v = 0\,\mathrm{m^2/s}$ (a) and $D_v = 10^{-2}\,\mathrm{m^2/s}$ (b) and with pressure (green) and no pressure included (blue)

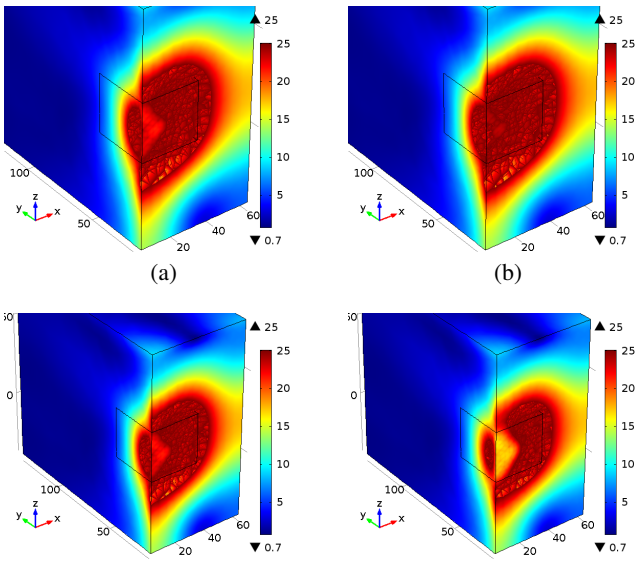

(a) (b) (c) (d)

Fig. 13 Von Mises [MPa] for $D_v = 0\,\mathrm{m^2/s}$ for $f = 1$ (a) and for $f = 0$ (b). Von Mises stress for $D_v = 0.01\,\mathrm{m^2/s}$ for $f = 1$ (c) and for $f = 0$ (d). All the domains with a Von Mises stress above 25 MPa are not shown. $f = 1$ means no evaporation, $f = 0$ means maximum evaporation

The Figs. 13(a) and 13(b) show the Von Mises stress inside the material without and with evaporation respectively. With evaporation, higher stress occurs in the center with values above 25 MPa, the material with stress above this limit is not represented. For the case of high diffusion (see Figs. 13(c) and 13(d), with $D_v = 0.01\ \mathrm{m^2}s$, the effect of evaporation leads to a distribution of the vapour content through the domain, lowering the total pressure. Hence, the total stress is lower in case of evaporation, the transport of heat from vapour decrease the thermal gradients and so the thermal stress. The comparison between Fig. 13(a) and 13(c) in the case of no evaporation or Figs. 13(b) and 13(d) in the case of evaporation shows that a larger diffusion coefficient lowers the total stress. For comparison, typical strength of normal Portland cement concrete are 2 to 5 MPa for the tensile strength and 20 to 40 MPa for the compressive strength.

Materials properties The real and imaginary part of the relative permittivity of the 3-D model are plotted in Fig. 14(a) and 14(b) respectively. The dry state with lower dielectric losses will absorb less microwave energy. The real part is in the range 5.4 to 6.5 and the imaginary part takes values from 0.46 to 0.68. These values are consistent with the measured permittivity of concrete samples (Soldatov *et al.*, 2013).

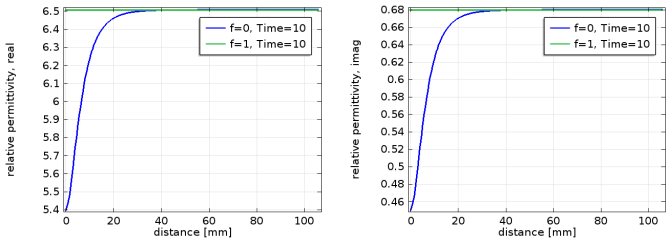

(a) ϵ^{real} (b) ϵ^{im}

Fig. 14 Relative permittivity for $D_v = 10^{-2}\,\mathrm{m}^2/\mathrm{s}$, real part (a) and imaginary part (b) with evaporation (green) and with no evaporation(blue)

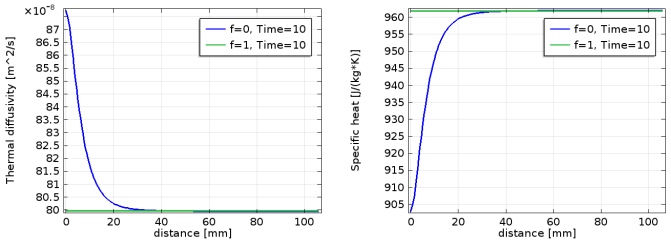

(a) κ (b) c

Fig. 15 Effective thermal diffusion [m^2/s] for $D_v = 10^{-2}\ \mathrm{m}^2/\mathrm{s}$ (a) and effective specific heat [$\mathrm{J}/(\mathrm{kg.K})$] (b) with evaporation (green) and with no evaporation (blue)

The Figs. 15(a) and 15(b) show the the variation of the thermal diffusivity and effective specific heat within depth for the 3-D model. As the surface is drying, less water content is present and the effective specific heat falls from 960 $J/(kg.K)$ (initial state) to 905 $J/(kg.K)$ (dry state).

5. CONCLUSION

A coupled multiphysics model based on heat an mass diffusion equations was developed in order to compute the total stress and to compare the thermal stress with the pore pressure. The deliberate use of constant and extremes values for the vapour diffusion coefficients is to facilitate the interpretation of the results and to help the understanding of the physical mechanisms involved during microwave heating of the porous concrete material. It was not possible to directly compare with experimental work, but the pressure values are consistent with literature and with the saturated vapour pressure. With a conical antenna operating at 2.45 GHz and an input power of 10 kW, the maximal temperature calculated near the surface are about 300 °C corresponding to temperatures measured experimentally. For this temperature, the calculated pore pressure is 9.5 MPa for the isochoric transformation (closed volume domain, no diffusion) and about 0.2 MPa with a large vapour diffusion coefficient $D_v = 0.01\ \mathrm{m}^2/\mathrm{s}$. The maximum Von Mises stress is in the range $28 - 37$ MPa and located about $7 - 8$ mm inside the concrete. From these first results, it seems clearly that the thermal stress is the dominant effect in case of explosive spalling of concrete with microwave heating. The pore pressure could play a role in triggering the spalling as suggested in the literature. It was observed experimentally that larger ablations occur in wet concrete than in dry concrete. One explanation could be that the microwave power density is higher in the case of wet concrete because of higher loss factor. The Spatial Reaction Engineering Approach used to calculate the water and vapour content distribution has the advantage of using a limited number of new parameters. Some large uncertainty exist for some parameters describing the porous medium such as the internal mass transfer coefficient $h_{m,in}$ or internal surface area A_{in}. In principle these parameters could be determined experimentally or estimated from the micro structure of the material. The relative activation energy was not available from experiment and therefore only two extreme cases were simulated, maximum and no evaporation. For further works, it would be useful to obtain this relative activation energy function. Secondly, a better estimation of the effective diffusion coefficient for liquid and vapour would be useful to improve the model. This is not a simple task because concrete under fast microwave heating is experiencing probably internal micro or macro cracks. The modification of the micro structure changes drastically the values of the diffusion coefficients. Finally, the calculated total stress exceeds the concrete strength and so these values are consistent with the apparition of the explosive spalling which occurs with our current antenna in the range from 3 to 10 s depending on the concrete initial water content and porosity.

NOMENCLATURE

q_0	peak power density (W/m^3)
β	attenuation constant for a plane wave ($1/\mathrm{m}$)
V_i	Volume of the phase i ($i = s, l, v, a$) (m^3)
ϵ_0	Porosity (-)
$f_i = V_i/V$	volume fraction of phase $i = s, l, v, a$ (-)
C_i	local concentration of phase $i = \{s, l, g, v, a\}$ (kg/m^3)
ρ_i	density of phase $i = \{s, l, g, v, a\}$ (kg/m^3)
ρ	effective density (kg/m^3)
X_i	mass content of phase $i = \{l, v, a\}$ (kg/kg dry)
D_l	liquid effective diffusivity (m^2/s)
D_v	vapor effective diffusivity (m^2/s)
I	Evaporating / condensation rate ($\mathrm{kg}/(\mathrm{s.m}^3)$)
$h_{m,in}$	internal mass transfer coefficient (m/s)
A_{in}	internal surface area ($\mathrm{m}^2/\mathrm{m}^3$)
ΔE_v	activation energy(J/kg)
ΔE_∞	equilibrium activation energy of the dry state (J/kg)
RH_∞	relative humidity of the dry state (-)
T_∞	temperature of hot air, dry state (K)
c	effective specific heat (J/kg · K)
c_i	specific heat of phase $i = \{s, l, g, v, a\}$ (J/kg · K)
k	effective thermal conductivity($\mathrm{W}/(\mathrm{m.K})$)
k_i	conductivity of phase $i = \{s, l, g, v, a\}$ the solid($\mathrm{W}/(\mathrm{m.K})$)
$C_{int,sat}$	internal saturated (or equilibrium) vapour concentration(kg/m^3)
$C_{v,sat}$	saturated (or equilibrium) vapour concentration (kg/m^3)
$\rho_{v,sat}$	saturated vapour (or equilibrium) density((kg/m^3)
I	source/depletion coupling term ($\mathrm{kg/s.m}^3$)
ΔH	latent heat of vaporisation of water (J/kg)
H	latent heat of vaporisation of water (J/mol)
σ	stress tensor (Pa)
σ_0	initial stress tensor (Pa)
E	Young modulus (Pa)
ν	poisson ratio (-)
α	linear expansion coefficient ($1/\mathrm{K}$)
M_v	molar mass of water ($\mathrm{kg}/\mathrm{kmol}$)
M_a	molar mass of air ($\mathrm{kg}/\mathrm{kmol}$)
R	Universal gas constant (J/kg K)
ϵ^{real}	real part of the relative effective permittivity
ϵ_i^{real}	real part of the relative permittivity of phase $i = \{s, l, g, v, a\}$
ϵ^{im}	imaginary part of the relative effective permittivity
ϵ_i^{im}	imag part of the relative permittivity of phase $i = \{s, l, g, v, a\}$
t_{heat}	time constant for the heat transfer model (s)
t_{diff}	time constant for diffusion model (s)
L	characteristic length (m)
κ	thermal diffusivity (m^2/s)

ACKNOWLEDGEMENTS

This research and development project is funded by the German Federal Ministry of Education and Research (BMBF) within the funding action "Decommissioning / dismantling of nuclear facilities " (funding number 02S8719) and managed by the Project Management Agency Karlsruhe (PTKA).

REFERENCES

Akbarnezhad, A., and Ong, K., 2011, "Thermal Stress and Pore Pressure Development in Microwave Heated Concrete," *Computers and Concrete*, **8**(4), 425–443.
http://dx.doi.org/10.12989/cac.2011.8.4.425.

Bazant, Z.P., and Goangseup, Z., 2003a, "Decontamination of Radionuclides from Concrete by Microwave Heating.1: Theory," *Journal of engineering mechanics*, **129**(7), 777–784.
http://dx.doi.org/10.1061/(ASCE)0733-9399(2003)129:7(777).

Bazant, Z.P., and Goangseup, Z., 2003b, "Decontamination of Radionuclides from Concrete by Microwave Heating.2: Computations," *Journal of engineering mechanics*, **129**(7), 785–792.
http://dx.doi.org/10.1061/(ASCE)0733-9399(2003)129:7(785).

Bazant, Z.P., and Thonguthai, W., 1978, "Pore Pressure and Drying of Concrete at High Temperature," *Journal of the engineering mechanics division*, **52**, 1059–1079.

Chen, X., 2007, "Moisture Diffusivity in Food and Biological Materials," *Drying technology*, **25**, 1203–1213.
http://dx.doi.org/10.1080/07373930701438592.

Chen, X., 2008, "The Basics of a Reaction Engineering Approach to Modeling Air-drying of Small Droplets or Thin Layer Materials," *Drying technology*, **26**, 627–639.
http://dx.doi.org/10.1080/07373930802045908.

Chen, X.D., and Putranto, A., 2013a, "Modelling Drying Processes, a Reaction Engineering Approach," *Cambridge University Press*.
http://dx.doi.org/10.1017/cbo9780511997846.

Chen, X.D., and Putranto, A., 2013b, "Spatial Reaction Engineering Approach as an Alternative for Nonequilibrium Multiphase Mass Transfer Model for Drying of Food and Biological Materials," *American Institute of Chemical Engineers*, **59**(1), 55–67.
http://dx.doi.org/10.1002/aic.13808.

Gawin, D., Pesavento, F., and Schrefler, B.A., 2011a, "What Physical Phenomena can be Neglected when Modelling Concrete at High Temperature? A Comparative Study. Part 1: Physical Phenomena and Mathematical Model," *International Journal of Solids and Structures*, **48**, 1927–1944.
http://dx.doi.org/10.1016/j.ijsolstr.2011.03.004.

Gawin, D., Pesavento, F., and Schrefler, B.A., 2011b, "What Physical Phenomena can be Neglected when Modelling Concrete at High Temperature? A Comparative Study. Part 2: Comparison between Model," *International Journal of Solids and Structures*, **48**, 1927–1944.
http://dx.doi.org/10.1016/j.ijsolstr.2011.03.003.

Incropera, F.P., and DeWitt, D.P., 1996, "Fundamental of Heat and Mass Transfer," 839–843. ISBN 0-471-30460-3.

Ju, Y., Liu, H., Tian, K., Liu, J., Wang, L., and GE, Z., 2013, "An Investigation on Micro Pore Structures and the Vapor Pressure Mechanism of Explosive Spalling of RPC Exposed to High Temperature," *Science China, technological science*, **56**(2), 478–470.
http://dx.doi.org/10.1007/s11431-012-5110-4.

Lepers, B., Soldatov, S., Link, G., and Jelonnek, J., 2013, "A Thermoelastic Model for Microwave Ablation of Concrete," *14th International Conference on Microwave and high frequency heating, Nottingham UK*.

Mindeguia, J., Pimienta, P., Noumowe, A., and Kanema, M., 2010, "Temperature, Pore Pressure and Mass Variation of Concrete Subjected to High Temperature- Experimental and Numerical Discussion on Spalling Risk," *Cement and Concrete Research*, **40**, 477–487.
http://dx.doi.org/10.1016/j.cemconres.2009.10.011.

Phan, L., 2008, "Pore Pressure and Explosive Spalling in Concrete," *Materials and Structures*, **41**, 1623–1632.
http://dx.doi.org/10.1617/s11527-008-9353-2.

Putranto, A., and Chen, X.D., 2013a, "Multiphase Modeling of Intermittent Drying Using the Spatial Reaction Engineering Approach (S-REA)," *Chemical engineering and processing*, **70**, 169–183.
http://dx.doi.org/10.1016/j.cep.2013.04.005.

Putranto, A., and Chen, X.D., 2013b, "Spatial Reaction Engineering Approach as a Multiphase Drying Approach to Model the Heat Treatment of Wood under a Constant Heating Rate," *Industrial and engineering Chemistry research*, **52**, 6242–6252.
http://dx.doi.org/10.1021/ie4000689.

Soldatov, S., Kayser, T., Link, G., and Jelonnek, J., 2013, "Temperature Dependent Dielectric Measurements of Concrete with Cavity Perturbation Method," *14th International Conference on Microwave and High Frequency Heating, Nottingham UK*.

Zhang, J., and Datta, A., 2004, "Some Considerations in Modeling of Moisture transport in Heating Hydroscopic Materials," *Drying Technology*, **22**(8), 1983–2008.
http://dx.doi.org/10.1081/DRT-200032740.

APPENDIX A

The saturated vapour concentration of water can be expressed from the Clapeyron Eq. (20) and the ideal gas law for vapour with the following expression:

$$\rho_{v,sat}(T) = \frac{M_v}{RT} p_{sat}(T)$$

Material properties

Electric permittivity For a 3-D model solving the wave equations and computing the power density distribution inside the sample, the relative permittivity depends on the water content inside the material. The relative real and imaginary part of the dielectric permittivity can be expressed as a function of the dry solid, the water, vapor and the air.

$$\epsilon^{real,im} = f_s \epsilon_s^{real,im} + f_l \epsilon_l^{real,im} + (f_v + f_a)\epsilon_g^{real,im}$$

with $f_i = \frac{C_i}{\rho_i}$ for $i = \{s, l, v, a\}$ the volume fraction of the solid, liquid vapour and air phase. The effective permittivity can be written as:

$$\begin{aligned} \epsilon^{real,im} &= \frac{V_s}{V}\epsilon_s^{real,im} + \frac{V_l}{V}\epsilon_l^{real,im} + \frac{V_g}{V}\epsilon_g^{real,im} \\ &= \frac{C_s}{\rho_s}\epsilon_s^{real,im} + \frac{C_l}{\rho_l}\epsilon_l^{real,im} + (1 - \frac{C_s}{\rho_s} - \frac{C_l}{\rho_l})\epsilon_g^{real,im} \end{aligned}$$

with $\epsilon_g^{real} = \epsilon_v^{real} = \epsilon_a^{real} = 1$ and $\epsilon_g^{im} = \epsilon_v^{im} = \epsilon_a^{im} = 0$. The measurement of different samples of dry concrete (no more free water) from Soldatov *et al.* (2013) have given the following range for the loss tangent and real part of the permittivity $0.01 < \tan\delta < 0.03$, $4 < \epsilon^{real} < 5$. This gives for the relative imaginary part $0.04 < \epsilon^{im} < 0.15$. For our simulations, the following permittivity was chosen for the dry concrete

Global Digital Central
ISSN: 2151-8629

$e_s = 4 - 0.08j$. The free water inside the concrete is in some degree bounded to the concrete, and for realistic concrete permittivity value range, the permittivity of the liquid phase has to be lower than the free water. It was set to $\epsilon_l = 30 - 6j$. The intrinsic temperature dependence of the dielectric properties is not taken into account in this present work.

Thermal properties

Density The effective density is the mass of all the constituents over the total volume:

$$\begin{aligned} \rho_{eff} &= \frac{m_s + m_l + m_v + m_a}{V} \\ &= C_s + C_l + C_v + C_a \end{aligned}$$

The concentration are related to the density of the substance with Eq. (4). For the dry concrete and water the density are $\{\rho_s, \rho_l\} = \{2400, 1000\}$ $\mathrm{kg/m^3}$. The density of vapour and air function of temperature and pressure was calculated with the ideal gas law.

Specific heat The specific heat is calculated from energy conservation below:

$$\begin{aligned} mc_{eff} &= m_s c_s + m_l c_l + m_g c_g \\ \frac{mc_{eff}}{V} &= \rho_{eff} c_{eff} = C_s c_s + C_l c_l + C_g c_g \\ c_{eff} &= \frac{C_s c_s + C_l c_l + C_g c_g}{\rho_{eff}} \end{aligned}$$

The specific heat c_g of the mixture vapour and air assuming an ideal gas, follows Dalton law:

$$\begin{aligned} c_g(T) &= \frac{n_a M_a}{n_a M_a + n_v M_v} c_a(T) + \frac{n_v M_v}{n_a M_a + n_v M_v} c_v(T) \\ &= \frac{m_a}{m_a + m_v} c_a(T) + \frac{m_v}{m_a + m_v} c_v(T) \\ &= \frac{C_a}{C_a + C_v} c_a(T) + \frac{C_v}{C_a + C_v} c_v(T) \end{aligned}$$

with m, the total mass, m_i the mass of the constituent i ($i = s, l, a, v$). C_i and c_i, $i = s, l, v, a$. n_i is the number of moles of the constituent i and M_i is the molar mass ($M_a = 29$ g/mol and $M_v = 18$ g/mol). are respectively the concentration and specific heat of the constituent i at constant volume. $C_g = C_v + C_a$ is the concentration of the gas. For an ideal gas, the specific heat is only function of temperature. $c_v(T)$ and $c_a(T)$ are linearly interpolated from thermodynamic table. $\{c_s, c_l\} = \{800, 4200\}$ J/(kg.K) for dry concrete and liquid water.

Thermal conductivity The effective thermal conductivity is defined in the same way as the specific heat and weighted with the mass fraction of its constituents.

$$\begin{aligned} k_{eff} &= \frac{C_s k_s + C_l k_l + C_g k_g}{\rho_{eff}} \\ k_g &= \frac{C_a}{C_a + C_v} k_a(T) + \frac{C_v}{C_a + C_v} k_v(T) \end{aligned}$$

with V_i , k_i and ρ_i the volume, thermal conductivity and density of the constituent i. $k_a(T)$ and $k_v(T)$ are defined from Incropera and DeWitt (1996). The thermal conductivity of the gas is defined according to the mass ratio of air and vapour. $\{k_s, k_l\} = \{1.7, 0.6\}$ W/(m.K).

Mechanical properties For the mechanical model, standard properties of normal Portland cement concrete were used. The following values for the young modulus, poisson ratio and linear thermal expansion coefficient were used. $\{E, \nu, \alpha\} = \{30$ GPa, 0.12, 10^{-5} 1/K$\}$

APPENDIX B

Ablation tests were performed on concrete blocs of $33 \times 40 \times 10$ cm with a conical antenna of input power 10 kW operating at 2.45 GHz. An air gap of 1 cm between the surface of the concrete and the aperture of the antenna avoids direct heat conduction from the concrete surface to the antenna. Explosive spalling depends of the water content and the type of the concrete. With our antenna explosive spalling occurs after 3 to 10 s of high power microwave heating depending on the input power and displacement rate of the concrete blocs(see Fig. 16(b)).

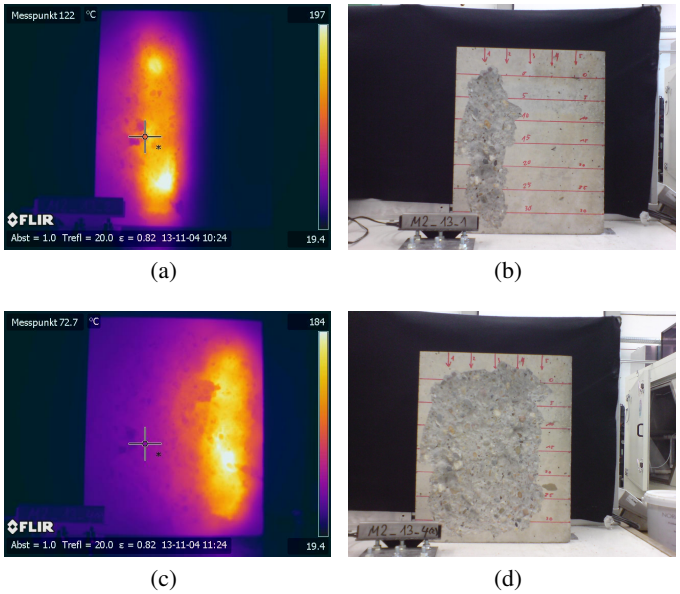

(a) (b)

(c) (d)

Fig. 16 Pictures of the surface ablation and temperature of the surface recorded with a thermo camera. The ablation time for one column takes about 30 s. Surface temperature was about $160-190\,^{\circ}$C after some seconds of air natural convection cooling. Temperatures in the range of $200-300^{\circ}$C have been recorded with a pyrometer